HVS (a hydrodynamic Valve): Enhancing Sucker Rod Pump Performance and Reducing Failure Rates in High-Angle Wellbores

C. Coyes[1]*, C. Jensen[2], J. Paez[3], B. Williams[4]

[1]Q2 Artificial Lift Services, Red Deer, Alberta, Canada
[2]Scribe Solutions Inc., Calgary, Alberta, Canada
[3]Q2 Artificial Lift Services, Red Deer, Alberta, Canada
[4]Q2 Artificial Lift Services, Red Deer, Alberta, Canada

*Author; email: ccoyes@q2als.com

Abstract

This study presents a performance evaluation of the HVS (a hydrodynamic system) to enhance downhole flow dynamics by generating vortex flow and applying an effective seal from 60° to 90° inclination. Laboratory experimentation under simulated downhole conditions was compared to HVS rod pumping field applications in the horizontal and build sections.

An acrylic transparent flow run, filled with water, simulated downhole conditions at three flow rates in horizontal and inclined positions. Media, such as air, nanobubbles, frac-sand and guar, were added to mimic downhole fluid. Pressure measurements were recorded, with and without the HVS, at steady state and with reciprocation, to measure sealing efficiency. Flow and pressure values were captured during each test run, and qualitative observations were recorded at visual fields. A review of HVS installations across North America targeted a study set in the Bakken. Field data over 5 years was compared to laboratory results.

Laboratory experiments and field deployments consistently demonstrate the HVS's effectiveness, particularly in high-angle wellbores. Controlled laboratory testing revealed reduced pressure fluctuations and the presence of organized vortex structures under simulated downhole conditions. Slow-motion recordings of fluid flow in the laboratory setting illustrated a 2-dimensional sinusoidal waveform, further validated by reciprocation tests that measured pressure signatures before and after the HVS—evidence of structured vortex flow. A hydrodynamic effect of the barbell firmly seated in the vortex insert was observed at the end of the reciprocation cycle. These hydrodynamic effects correlate with field observations, where the HVS maintained stable operation at inclinations between 55° and 70°. Field data from 14 wells lowered on average 722 ft deeper into the wellbore to an inclination of 70° showed a 143.5% increase in total fluid production.

The results challenge the conventional use of ball-and-seat valve systems, highlighting the HVS as a promising alternative for reciprocating pump applications. It underscores the HVS's capability to optimize sealing, enhance flow in deviated wellbores, and suggest a potential reduction in pump failure frequency, post-HVS installation, in high-angle environments. The study opens new avenues for leveraging hydrodynamic sealing mechanisms to enhance reliability and performance.

Introduction

Low pump efficiency is a persistent, well-documented, and costly problem in sucker rod pumps ultimately causing mechanical repair, downtime, and/or mitigative operational strategies. The challenges with sucker rod pumps have a lengthy history. Connally, Sandberg, and Stein (1953) explored the causes of low volumetric efficiency. They stressed the negative impact of gas interference while emphasizing the importance of efficient valve action.

In modern production environments, most wells are drilled horizontally to extend reach deeper into reservoirs and enhance horizontal extraction techniques. Deeper and longer horizontal wells are further complicated by downhole environments with high gas-oil ratios creating gas interference, causing erratic flow behavior and contributing to low sucker rod pump efficiency. Landing sucker rod pumps as deeply as possible increases fluid head level and maximizes production. The strategy of landing pumps in curved sections, closer to the horizontal pay zone, has evolved production strategies. Kolawole et al. (2019) documented a comprehensive review of common challenges when attempting to pump in the build and horizontal section of the wellbore. They noted issues with fluctuating multi-phase flow, solids and gas interference, and increased mechanical failure frequencies.

Within the sucker rod pump system, the standing and traveling valves serve critical roles in maintaining the fluid flow. Aslanov (2024) noted that the high differential pressures across valves require reliable sealing between the ball and the seat. Operators are familiar with persistent wear, which, even minor flaws in the sealing surfaces, compounded by corrosion and wear, can lead to increased failure, necessitating servicing and causing production downtime. This is amplified by landing the sucker rod pump deeper in the curve at higher angles.

Research efforts into fluid flow behavior offer a way to approach these cumulative challenges in the curved sections of downhole environments. Mingaleeva's (2002) exploration of fluid dynamics revealed the significance of the helical motion of fluids in sharp bending paths. It describes how a vortex overcomes hydraulic drag in a bending path, suggesting vortex flow potential in downhole environments. Jalikop, et al.'s (2020) study used a computational fluid dynamics model to understand fluid flow inside the standing and traveling valve to determine critical flow and optimal operating parameters for sucker rod pumps.

Vortex designs in downhole applications are an expanding area of research and field trials. Luo et al. (2019) conclude from their review of liquid unloading by vortex tools that there is benefit in the application of vortex tools, but more research is needed. Zhou et al. (2019) studied two-phase vortex flow through a liquid film dynamic analysis model to optimize vortex tools and test in the field. It concluded that vortex flow created from an optimal helical angle contributes to upward flow, improving carrying capacity. Coyes et al. (2023) examined the use of a vortex insert in a laboratory environment and compared it to its use in the field. Their experiment established how specialized vortex geometry contributed to stabilized flow around the ball valve, reducing ball chatter, increasing flow and extending run life. These studies and field trials suggest vortex applications downhole stabilize the fluid flow profile and increase flow velocity, thereby increasing pump efficiency.

This paper explores the challenge operators face when sucker rod pumps are landed beyond inclination limitations of the standing and travelling valves. The experiment and field study in this paper were designed to explain field production efficiencies realized with a downhole vortex system, the Hydro Dynamic System (HVS), through a series of laboratory experiments and analysis of field data. Laboratory testing in a transparent acrylic flow run was designed to simulate field and downhole conditions of the HVS in horizontal and inclined orientations. It examined pressure fluctuations and observed flow in various simulated downhole artificial lift conditions: small gas particulates, guar and frac sand, reciprocation.

Vortex flow downhole devices have been implemented in field operations and studied in laboratory analysis to show how vortex fluid flow can decrease pressure drop and increase flow to extend run life. One such system was designed with a spherical velocity profile that cups the ball in place, stabilizing the velocity profile in the smallest cross-sectional area of the pump to eliminate ball vibration while fluid passes. Stabilized flow through this vortex insert increased fluid flow through constricted space while reducing frictional energy in the valve (Coyes et al. 2023).

The application of these vortex devices creates a vortex flow where kinetic energy builds in the smallest area of the pump, increasing velocity during each pump stroke. If gas is in solution below the standing valve, as fluid moves past the ball, the gas stays in the liquid state, passes through the vortex geometry and enters a vortex above the ball. The resulting swirl flow above the insert maintains the gas in solution limiting the potential for fluid pound due to gas breakout at a gas-liquid interface that can be problematic in sucker rod pumps. **Fig. 1** below illustrates the axial upward flow through the spherical cross-sectional area of a vortex insert. With a device that establishes a downhole vortex flow, the next challenge was to sustain the vortex flow to keep gas entrained and suspend solids further along the flow path.

Fig. 1—Stabilized flow through vortex insert.

Hydro Dynamic System (HVS)

The Hydro Dynamic System, or HVS, is a unique valve design that features vortex geometry with two balls joined by a connecting stem, instead of a single ball that seals against a seat (**Fig. 2**). The barbell geometry and the tapered seat have a larger surface area than conventional ball and lapped seats. The HVS uses pressure differential to ensure sealing action. This innovative barbell shape uses the combination of back pressure pulse at the end of the reciprocation cycle, the hydrodynamic force of the cage geometry, and the pressure at well depth to close the valve. The hydrodynamic force pushes the barbell shape into a tapered seat, enabling valve sealing action on each stroke and improving pump efficiency at high inclinations.

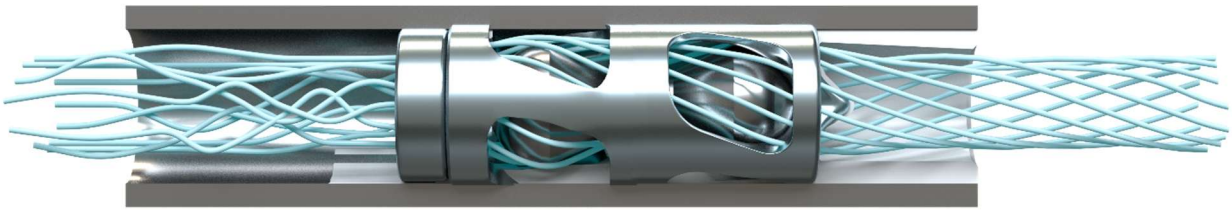

Fig. 2—Hydro Dynamic System including cage or casing, seat, barbell, and vortex insert.

Like conventional standing and traveling valves, the HVS functions with a reciprocating motion. As shown **Fig. 3**, during the upstroke (moving right in the figure), the HVS traveling valve closes while the standing valve opens, allowing fluid to enter the pump barrel. On the downstroke, the traveling valve opens and the standing valve closes, transferring the fluid above the traveling valve into the production column for delivery to the surface.

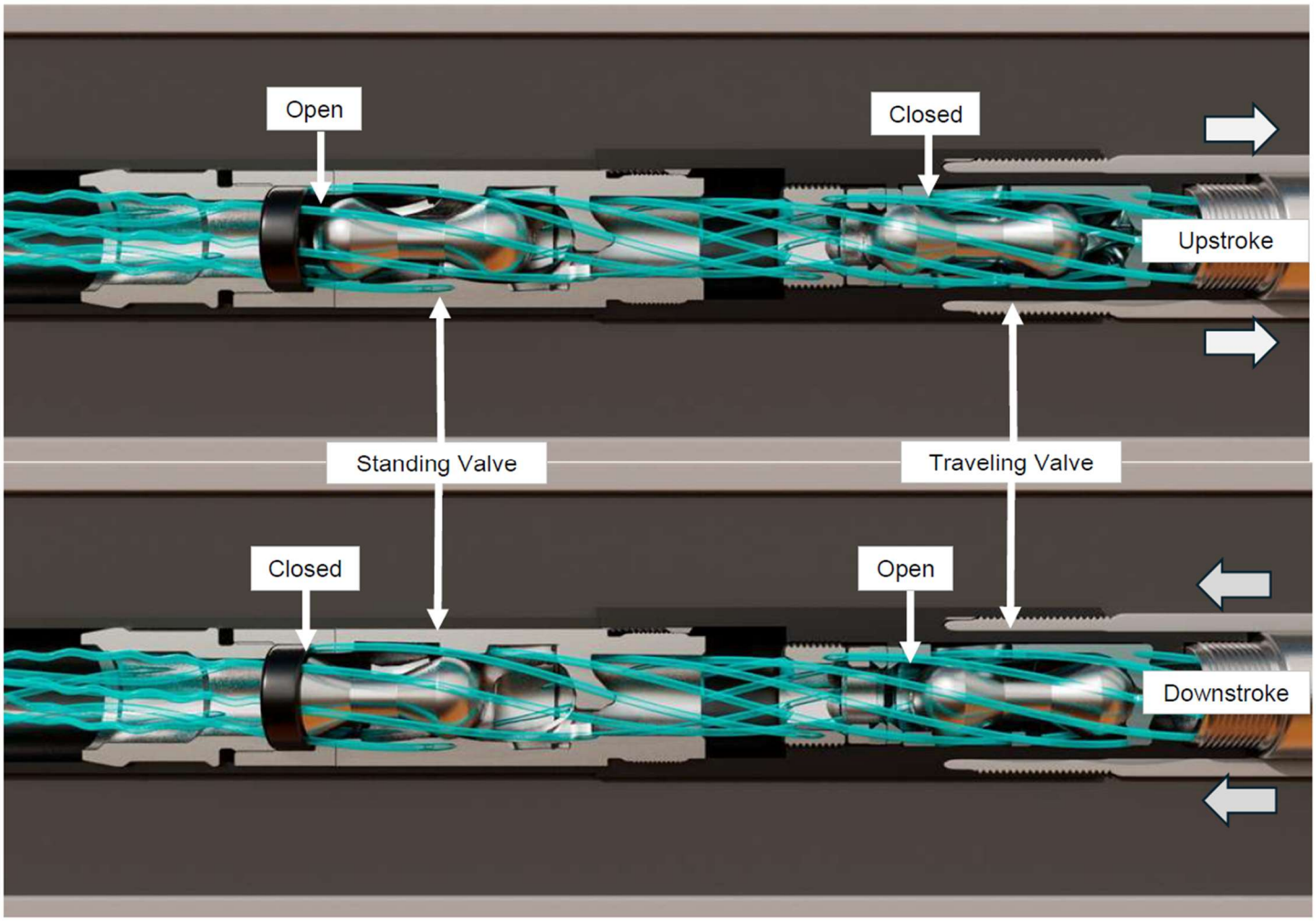

Fig. 3—Upstroke: Standing valve open, traveling valve closed, fluid into barrel chamber; Downstroke: Standing valve closed, traveling valve open, fluid into hydrostatic fluid column.

Laboratory Testing

The laboratory testing aimed to observe fluid flow behavior through the HVS under simulated downhole conditions and to gather data to measure nodal pressure fluctuations and pressure drop along the flow line. Downhole conditions were simulated using a variety of media, flow rates, and reciprocation. Air and nanobubbles (NB) were injected to create a visual tracer of flow patterns so flow could be qualitatively observed.

The following testing objectives were set out to support an understanding of HVS fluid flow under simulated downhole conditions:

1. Measure pressure differentials and fluctuations by varying pump speed.
2. Compare results from baseline (no valve) and with the HVS valve.
3. Trial a variety of media: reverse osmosis (RO) water, gas, guar and sand.
4. Test HVS performance at 90° and 60° (simulated pumping in the curve).
5. Calculate pressure drop from pressure sensor data.
6. Simulate reciprocation to gather data on the HVS function.
7. Qualitatively observe the flow patterns for velocity vectors inside the flow regime with and without gas.

Lab apparatus

A laboratory apparatus was designed and constructed to investigate the performance of the HVS under simulated downhole conditions (i.e., gas and/or solids entering the HVS). The lab apparatus was assembled and operated in a climate-controlled building to maintain the tank water temperature of 69.6°F and a filled flow run line water temperature of 70.6°F.

Appendix A: **Fig. A1** and Appendix B: **Fig**. **A2** illustrate a detailed schematic of the laboratory apparatus[1] and each includes a table (**Table A1**and **Table A2**) that provides distances between sensors and measured locations of the valve placement for the horizontal and inclined runs. Appendix C: **Table A3** details the equipment components used in the testing flow run, including the product name, manufacturer and technical specifications.

The laboratory apparatus was a linear arrangement to support flow through clear acrylic tubing that made up the flow run and return flow line. It was comprised of a nanobubble generator joined to a water tank and then connected to a water pump. A programmable logic control (PLC) interface was attached to the water pump to control and record the flow rate. The bottom of the water tank and pump were kept level with the flow run to avoid the effects of hydrostatic head on the pressure readings.

Tubing exiting the water pump was connected to inlets in sequence, including an air bleeder, an air purge system, and an export port. An air injector with a regulator controlled the atmospheric flow of air into the system and incorporated a solenoid to calibrate pressure. Gas was measured with pressure only. There was no Coriolis meter on the flow run to measure density. At 50 psi on the air solenoid gauge, a visual inspection through the acrylic pipe estimated 1-10% gas and 90 to 99% water by volume. The air bleeder, located directly above the pump, acted as a pressure relief valve. The air purge system was placed next to the air bleeder to clear the flow run between test runs.

Six-foot lengths of acrylic pipe were coupled with aluminum compression fittings to make up the flow run. The tubing maintained a consistent ID throughout (ID of 2.5 in. and OD of 3.0 in.). A 12-inch-long interchangeable piece of tubing was set at the valve location to swap out a blank (no valve) used for baseline testing and insert the HVS. The ID increased (3.58 inches) at the HVS installation location.

Six pressure sensors set along the entire length of the tubing were connected to the PLC. The pressure sensors were tapped into the aluminum couplings. The valve location was set between pressure sensors 2 and 3 for the horizontal flow run orientation and between pressure sensors 5 and 6 for the inclined flow run orientation. Eight visual fields were located halfway between each pressure sensor and 6 in. on either side of the valve location. Four pipe stands supported the tubing placed every 6-12 ft. A series of adjustable pulley systems elevated the flow run 19 ft from horizontal to run tests at an incline of 60° from vertical. A flow rate meter was placed at the end of the flow run to measure the actual flow rate and compare it against the theoretical flow rate at the pump. Testing occurred in two flow run orientations: 90° (horizontal) and 60° from the vertical (inclined).

The first phase of testing used reverse osmosis water (RO) in the system. The entire system, when filled, held 241.7 gallons of RO: tank - 211.3 gallons, piping system – 30.4 gallons. The fluid initially introduced into the water tank was continuously cycled for the entire experiment. The room was darkened during testing, and the flow run was illuminated with green LED lighting to enhance observation. Three green lasers (see Appendix C: **Table A3** for product specifications) located at each visual observation field were installed with a calibration guide to maintain a constant distance of 1.67 in. between the lasers. A consistent lateral distance of 8.5 in. between the flow run and the video camera lens was set to assure consistency at reading locations. NB were injected as an additional medium and acted as a supplemental visual tracer to see fluid flow patterns as fluid passed through the transparent flow run. When NB were introduced, the nanobubble generator injected NB to saturation into the water. The lasers illuminated bubbles in flow patterns and acted as reference points. (See **Fig. 4.**)

[1] Refer to Supplementary Materials Video S-1 Lab Apparatus.

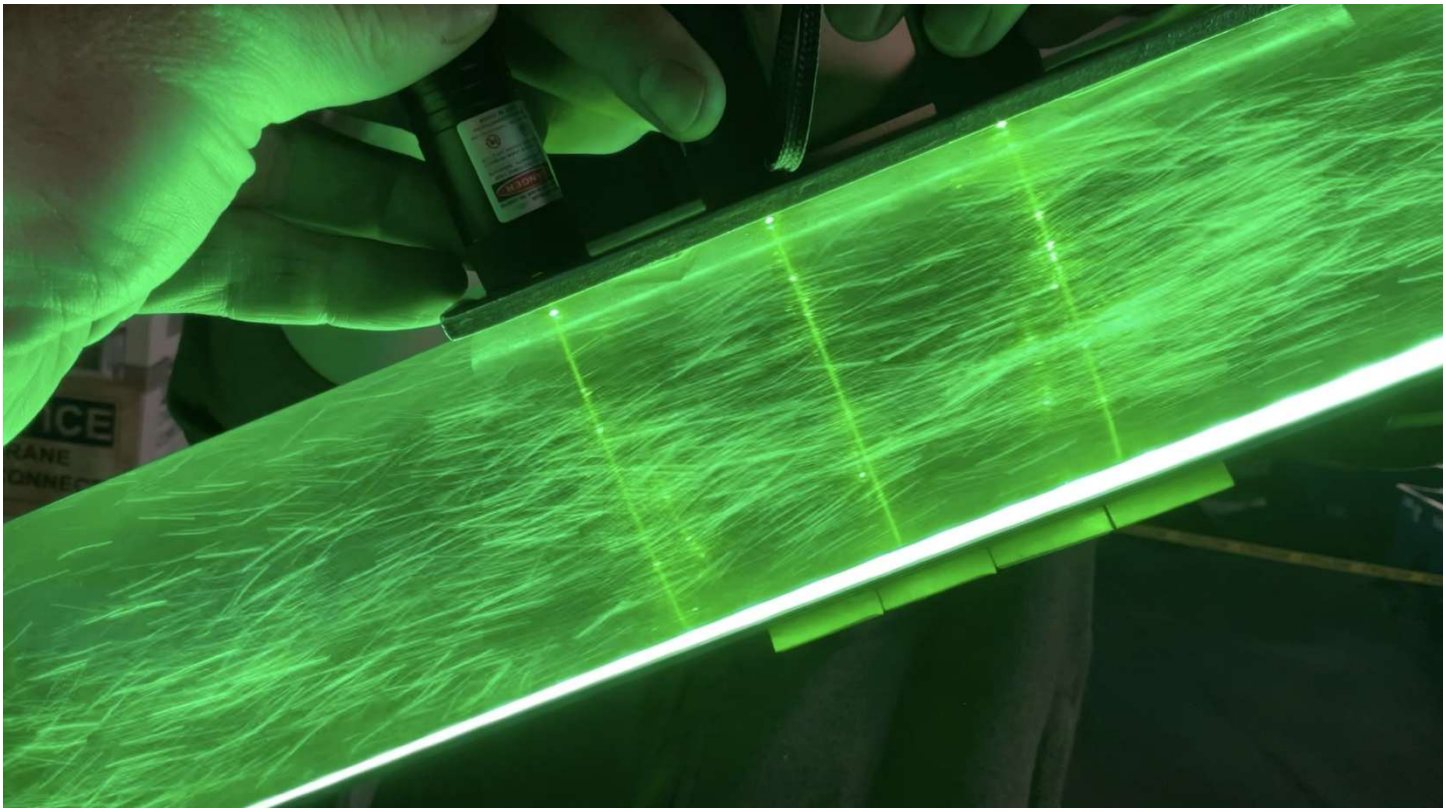

Fig. 4—Example of the flow run with bubbles at visual field 7 at 60°.

Understanding and generating nanobubbles (NB)

NB were primarily injected into the water tank to show visual flow profiles and observe fluid behavior in the transparent acrylic tubing. Additionally, it was speculated that NB may more closely resemble entrained gas in deep wells to approximate downhole pressure characteristics of entrained gas in the flow run.

It is challenging to achieve downhole pressures at surface, especially using clear acrylic tubing instead of steel pipe. Acrylic tubing has a pressure rating of up to 100 psi. Downhole conditions at 10,000 ft of hydrostatic pressure are equal to 4330 psi (with water). According to ideal gas law, gas under pressure gets smaller; therefore, injecting NB would more closely mimic downhole pressure conditions at surface.

In the research, NB are considered gas-filled cavities (bubbles) that are less than a micron. There are significant differences in the physicochemical properties depending on the gas and the aqueous solution at around 350 nm and smaller. The changes include buoyancy, uniform surface charge (negative), stability for long duration (days, weeks, indefinite), and in large quantities the ability to decrease viscosity, density (0.988 g $\times$ cm^3), zeta potential, ionic potential, and induce on surfaces a reduction in turbulence and a reduction in friction by forming a double slip layer at the boundary level. (Ohgaki et al.2010; Walke and Sathe 2012)

The nanobubble generator provider completed equipment verification of their equipment at Northwestern University's International Institute for Nanotechnology in Evanston, Illinois. Measurements confirmed the production of NB over a 20-minute timeframe. The verification process was completed with air and O_2 at 100, 150, 200, 250 and 300 psi. Density was quantified in the verification test by measuring the ppm of dissolved oxygen and converted to kg/m^3. Refer to detailed verification results on Unit L6 in **Appendix D** and **Fig. A3**.

Zhou et al. (2021) reviewed several methods for nanobubble detection in a fluid, including using a laser. Due to the Tyndall effect, laser beam light is scattered by particles in a medium. In this case, the green LED lights and high-powered green lasers illuminated NB and air bubbles in suspension. Therefore, a laser illuminated flow patterns, making the NB and air bubbles visible for qualitative observation. This effect can be seen in several examples throughout this paper: **Fig. 4**, **Fig. 9a and b**, **Fig. 10**, **Fig. 11**. When the videos with NB and without NB were compared, videos with NB had a distinct difference. When NB were present, the lasers illuminated a visible cloud effect.[2]

Methodology

The laboratory flow run experiment was conducted over three weeks, with approximately 170 experimental hours. The tank was filled with reverse osmosis water (RO) once, and the same RO was circulated and used for each run.

The experiment included a total of 48 runs. **Table 1** and **Table 2** below summarize details for each run in the horizontal and incline orientations. For each run, the media type added, volumetric flow rate and pump rate were recorded. Runs were completed in three groups with volumetric flow rates of 100%, 85%, 70% and theoretical pump speeds of 70, 59.5, and 49 gal/min, respectively. At each pump rate, the pump was initiated and run until a consistent flow was achieved, then observations were captured. Pressure sensor readings were taken for each run to calculate an average and standard deviation. An 8-second slow-motion video was recorded for qualitative analysis between the pressure sensors and the valve location at every visual observation field.

Injection of air, NB and additional media were recorded on runs noted in **Table 1** and **Table 2**. These media additions were added before readings were taken. The first 12 runs were completed with tubing at 90° in a horizontal orientation. The remaining 36 runs were at a 60° incline from vertical.

The first nine runs acted as baseline runs with no HVS installed. Runs 1, 2 and 3 were run continuously with RO and pump speed changes. Atmospheric air was injected continuously at 50 psi through the air injector (see Appendix A) for Runs 4, 5, and 6. After Run 6, NB were added. The flow line was cleared to return all fluid to the tank before injecting NB. For this experiment, Nanobubble Generator Unit L6 was used to generate NB into the water tank. The NB generator was run for 2 hours to ensure NB saturation into the water tank. With data provided from NB generator verification testing, this is equivalent to 999.997 kg/m^3 (refer to Appendix D for details). NB saturated in solution is a rounding error (nearly 1000 kg/m^3) with respect to the density of water. NB were injected into the system once and remained stable in solution for the entire experiment.

With the addition of NB, three more horizontal baseline runs were completed (Runs 7, 8, 9) at the three flow rates (100%, 85%, 70% pump speed) before the HVS was installed. After Run 9, the flow run was cleared, all fluid returned to the tank, and the HVS was installed in the pre-designated slot between pressure sensor 2 and pressure sensor 3. Three runs were completed (Runs 10, 11, 12) with the HVS and the tubing still in the horizontal orientation.

Between Run 12 and Run 13, the flow line was cleared, all fluid returned to the tank and the tubing was elevated 19 ft to 30° from the horizontal or 60° from the vertical. The HVS was moved to the curved section between pressure sensors 3 and 4 to represent pumping in the curve. Pressure sensor locations were adjusted (see sensor locations in Appendix B). Refer to the test matrix in **Table 2** for details about runs completed on incline. The remaining runs (13-48) were completed with inclined tubing. Runs 13 to 18 progressed in a steady state in two rounds of three, first with RO and NB and the second round (Runs 16-18) with RO, NB, plus additional atmospheric air.

After Run 18, the flow run was cleared, and all fluid returned to the tank. The PLC was programmed to simulate reciprocating stroke lengths, repeating full stop-Vmax-full stop. Once continuous reciprocation was established, Runs 19-24 were completed with the same recordings as Runs 13-18. After Run 24, the flow run was cleared, and all fluid returned to the tank. The final runs added 0.11 lb/gal of 16:40 frac sand suspended with alpha guar gum at a concentration of 0.006 lb/gal to suspend the frac sand and mimic downhole rheological properties in the flow run. Runs 25-30 were completed at steady state with additives—three with RO and NB, three runs with RO, NB and air. Runs 31-36 were completed with reciprocation and additives, three runs with RO and NB and three with RO, NB and air. After Run 36, the flow run was cleared, and all fluid returned to the tank. Pressure sensors were shifted to the underside of the tubing to measure differences between pressure valves and fluctuations between the top and bottom of the tubing. The final runs (37-48) were run with six in steady state and six with reciprocation.

[2] Refer to Supplementary Materials Video S-2 With and Without Nanobubble Cloud.

Flow Run Test Matrix

Table 1 and **Table 2** below summarizes testing variables for each run in the horizontal (90°) and inclined (60°) orientations.

	Run No.	Media type added	Volumetric Flow Rate % Pump Speed	Theoretical Pump Rate at the Pump (gal/min)	Atmospheric injection rate (psi)
Baseline Horizontal	Run 1	RO	100	70	
	Run 2	RO	85	59.5	
	Run 3	RO	70	49	
	Run 4	RO + air	100	70	50
	Run 5	RO + air	85	59.5	50
	Run 6	RO + air	70	49	50
	NB Added				100
	Run 7	RO + NB	100	70.0	
	Run 8	RO + NB	85	59.5	
	Run 9	RO + NB	70	49.0	
Flow run cleared, HVS installed					
HVS Horizontal	Run 10	RO + NB	100	70.0	
	Run 11	RO + NB	85	59.5	
	Run 12	RO + NB	70	49.0	
Flow run cleared, inclined					

Table 1—HVS laboratory test matrix – horizontal.

	Run No.	Media type added	Volumetric Flow Rate % Pump Speed	Theoretical Pump Rate at the Pump (gal/min)	Atmospheric injection rate (psi)
Incline HVS Steady State	Run 13	RO + NB	100	70.0	
	Run 14	RO + NB	85	59.5	
	Run 15	RO + NB	70	49.0	
	Run 16	RO + NB + air	100	70.0	50
	Run 17	RO + NB + air	85	59.5	50
	Run 18	RO + NB + air	70	49.0	50
Flow run cleared, PLC programmed for reciprocation					
Incline HVS Reciprocation	Run 19	RO + NB	100	70.0	
	Run 20	RO + NB	85	59.5	
	Run 21	RO + NB	70	49.0	
	Run 22	RO + NB + air	100	70.0	50
	Run 23	RO + NB + air	85	59.5	50
	Run 24	RO + NB + air	70	49.0	50
Flow run cleared, frac sand (27 lb, concentration - 0.11 lb/gal) and guar added (3.66 lb, concentration - 0.006 lb/gal)					
Incline HVS Steady state, Frac sand and guar	Run 25	RO + NB	100	70.0	
	Run 26	RO + NB	85	59.5	
	Run 27	RO + NB	70	49.0	
	Run 28	RO + NB + air	100	70.0	50
	Run 29	RO + NB + air	85	59.5	50
	Run 30	RO + NB + air	70	49.0	50
Flow run cleared, PLC programmed for reciprocation					
Incline HVS Reciprocation, Frac sand and guar	Run 31	RO + NB	100	70.0	
	Run 32	RO + NB	85	59.5	
	Run 33	RO + NB	70	49.0	
	Run 34	RO + NB + air	100	70.0	50
	Run 35	RO + NB + air	85	59.5	50
	Run 36	RO + NB + air	70	49.0	50
Flow line cleared, pressure sensors moved to bottom of tubing					
Incline HVS Bottom pressure sensors Steady state Frac sand and guar	Run 37	RO + NB	100	70.0	
	Run 38	RO + NB	85	59.5	
	Run 39	RO + NB	70	49.0	
	Run 40	RO + NB + air	100	70.0	50
	Run 41	RO + NB + air	85	59.5	50
	Run 42	RO + NB + air	70	49.0	50
Flow run cleared, PLC programmed for reciprocation					
Incline HVS Bottom pressure sensors Reciprocation Frac sand and guar	Run 43	RO + NB	100	70.0	
	Run 44	RO + NB	85	59.5	
	Run 45	RO + NB	70	49.0	
	Run 46	RO + NB + air	100	70.0	50
	Run 47	RO + NB + air	85	59.5	50
	Run 48	RO + NB + air	70	49.0	50

Table 2—HVS laboratory text matrix – incline.

Data Capture

Once continuous flow was established, the PLC recorded readings every second at each pressure sensor for each run. The pressure differential was calculated among these readings, averaged, and a standard deviation was calculated. Standard deviation was used to quantify the pressure fluctuation, or the pressure variability over time, at the tubing wall. A smaller standard deviation indicates lower friction on the tubing wall, supporting the presence of vortex flow. Higher standard deviation numbers indicate higher friction or turbulence at the tubing wall. Eight-second slow-motion videos were taken in sequence along the flow run during each run and reviewed for qualitative analysis at the six visual observation zones. Researchers watched a playback of the flow to observe flow patterns.

The experiment used two types of data capture: digital measurements from the PLC and digitally logged visual observations.

Digital measurements

Digital measurements were recorded from the PLC interface and downloaded from the PLC SIM card to an Excel spreadsheet for analysis. Each Run had a separate worksheet in the Excel workbook. Measurements and digital techniques are summarized below:

- PLC pressure sensor readings lengthwise and along cross-sectional areas of the tubing
- PLC volume and flow rate assessment (steady state and reciprocation)
    - Note. The flow rate device was located on the return line to measure the flow rate.
- Temperature of the tank and flow run with a temperature gun.
- Atmospheric injection rate sustained at 50 psi with gauge (when air was injected into the system)
- Total volumetric calculation of the entire system

Digital Observations Collected

Digital observations included:

- Stations equipped with green LED lighting, dark backdrop, and high-powered green lasers moved section by section.
- Video stations recorded 8-second slow-motion videos to capture flow behavior for flow pattern analysis. Over 200 video clips were recorded, categorized, labelled and analyzed.
- Qualitative analysis was gathered on the corresponding worksheet for each flow run.

Laboratory Data and Observation Results

Results were gathered from digital measurements and observations to support an understanding of HVS fluid flow under simulated downhole conditions. The results below show data compilations that support the testing objectives and focus on findings to determine vortex flow efficiencies in downhole environments that improve pump efficiency.

Horizontal Valve

During reciprocation testing, a hydrodynamic effect was observed**. Fig. 5** shows the end of the reciprocation cycle, where a back-pressure pulse of the barbell inside the HVS in the open position overcomes inertia. Then, a high-pressure to low-pressure differential facilitated by the valve cross-sectional area geometry pushes, seats, and seals the HVS, so no hydrostatic pressure is required to close the valve at 90°.[3]

[3] Refer to Supplementary Materials Video S-3 Hydrodynamic valve.

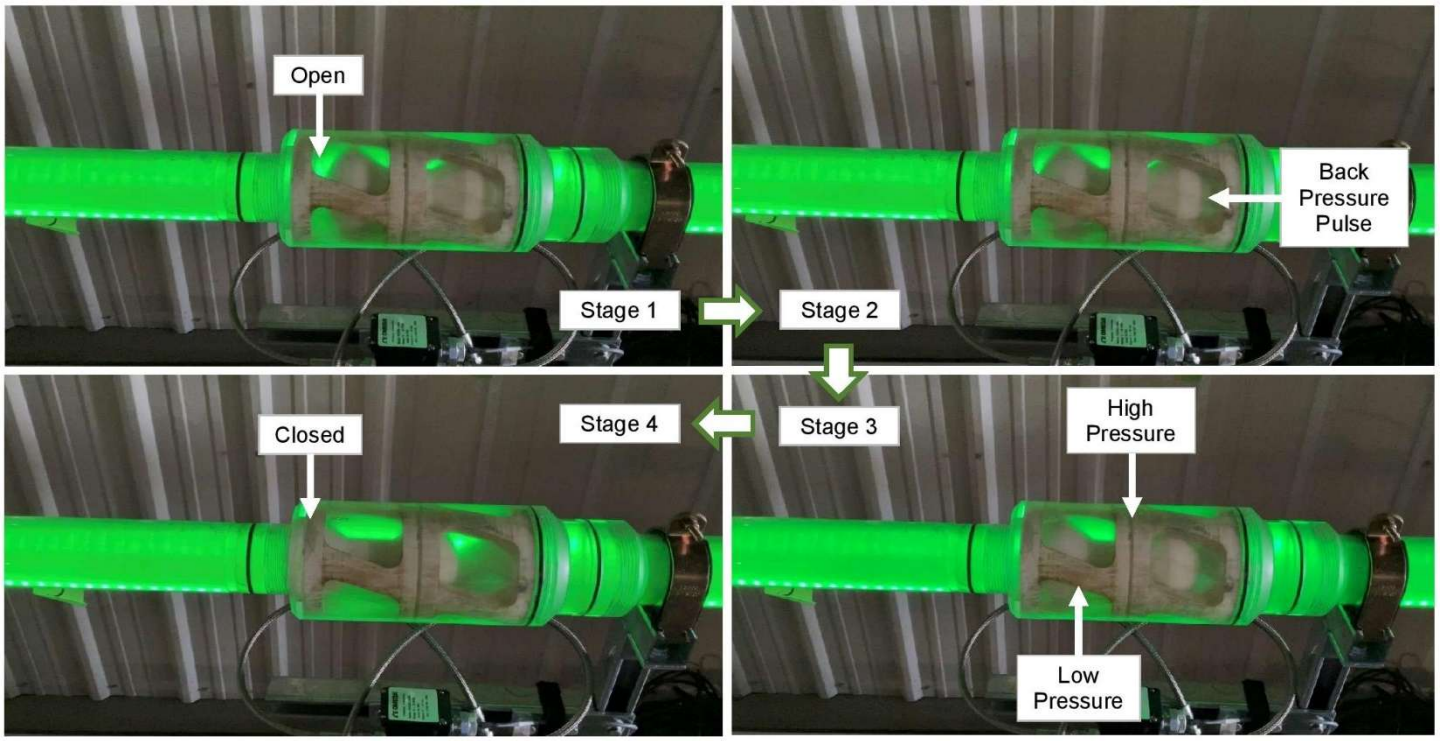

Fig. 5—Horizontal valve stages.

Baseline data versus HVS pressure readings

Baseline data (with no valve) versus HVS valve data surfaced expected results. With the flow run in the horizontal position, data from pressure sensors, placed on the top of the tubing wall, situated on either side of the valve location, were compiled for tested flow rates and multiphase flow and graphed for Runs 1-12. **Fig. 6** below illustrates the average pressure before the valve location (blue bars) and after the valve location (orange bars). The most significant average differentials are for readings with the HVS and NB; the largest differential is at 100 % flow rate with the HVS and NB at 1.63.

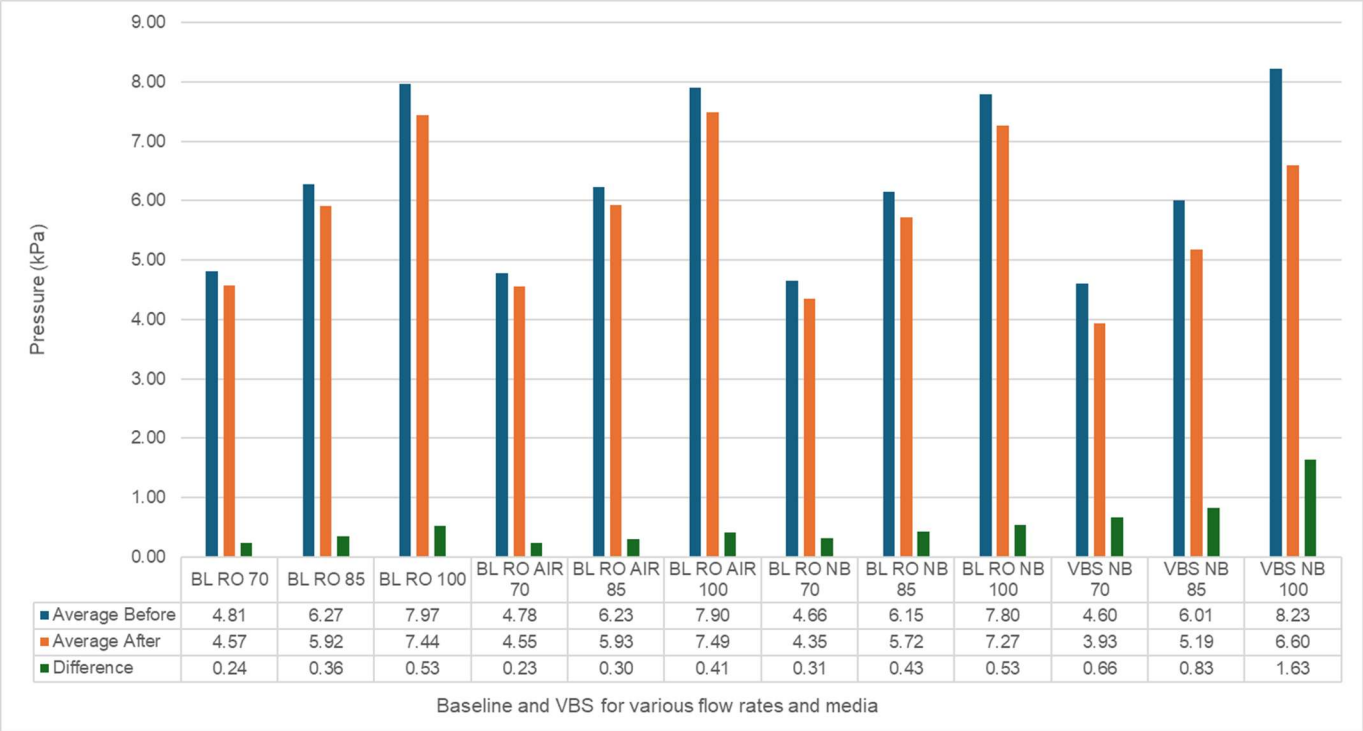

	BL RO 70	BL RO 85	BL RO 100	BL RO AIR 70	BL RO AIR 85	BL RO AIR 100	BL RO NB 70	BL RO NB 85	BL RO NB 100	VBS NB 70	VBS NB 85	VBS NB 100
Average Before	4.81	6.27	7.97	4.78	6.23	7.90	4.66	6.15	7.80	4.60	6.01	8.23
Average After	4.57	5.92	7.44	4.55	5.93	7.49	4.35	5.72	7.27	3.93	5.19	6.60
Difference	0.24	0.36	0.53	0.23	0.30	0.41	0.31	0.43	0.53	0.66	0.83	1.63

Baseline and VBS for various flow rates and media

Fig. 6—Average pressure on nodes before and after the baseline vs HVS at various flow rates and multiphase flow.

As expected by Bernoulli's equation, a constriction in the flow path causes a larger pressure drop, explaining the 1.63 kPa at HVS compared to the 0.53 kPa at baseline (**Fig. 6**). **Table 3** below describes the reduction in cross-sectional area that accounts for the larger pressure drop with the HVS. The HVS's smallest cross-sectional area takes up about ⅔ (64%) of the flow path.

	OD (in.)	ID (in.)	Area (in.^{2})	Thickness x Width (in.^{2})
Tubing	3.00	2.50	4.91	
Tubing at valve insert location	4.00	3.58	10.09	
HVS Insert	3.58	2.60		
HVS Insert Ribs (3 ribs)			1.39	0.46
Barbell (0.060 in. diameter clearance between HVS insert and barbell)	2.54		5.07	
Open flow area (Open flow area = Area of tubing at valve insert location – HVS insert ribs – barbell)			3.63	
Constriction (Area of constriction = area of tubing at valve insert location – open flow area)			6.46	
Percentage of HVS constriction in the open flow area = (Constriction / Area of tubing at valve insert) x 100			64%	

Table 3—HVS cross-sectional area and constriction.

Nodal pressure fluctuations during steady state fluid flow

Steady state measurements were taken at pressure nodes located on the top of each aluminum coupling. Each node was inset an ⅛ in. up from the ID of the flow run, to measure pressure fluctuations continuously. Steady state fluid flow analysis showed higher pressure fluctuation before the HVS and lower pressure fluctuation after the HVS. **Table 4** lists the standard deviation, measured in kPa, between pressure node fluctuations for baseline runs and fluctuations after the HVS was installed in the horizontal position (Runs 1-12). The pressure fluctuation values graphed in **Fig. 7** were determined by subtracting the standard deviation of pressure fluctuations after the HVS from the standard deviation of pressure fluctuations before the HVS.

The HVS RO NB column shows lower values, indicating lower friction at the tubing wall. Most significantly, the fluctuation calculation at 100% flow shows -0.65 kPa with the HVS, RO and NB. These lower frictional values suggest vortex flow, while higher numbers seen in baseline runs indicate higher friction and turbulent flow at the ID of the tubing wall.

% Flow	BL RO	BL RO Air	BL RO NB	HVS RO NB
70 %	0.47	0.40	0.42	0.12
85%	0.41	0.41	0.26	-0.18
100%	0.35	0.37	0.32	-0.65

BL=baseline, RO=reverse osmosis water, NB=nanobubbles, HVS=Hydro Dynamic System

Table 4—Pressure fluctuation across the valve.

When transposed to a graph, as shown in **Fig. 7**, runs with the HVS and NB have far fewer pressure fluctuations than baseline runs, especially at 100% flow rate.

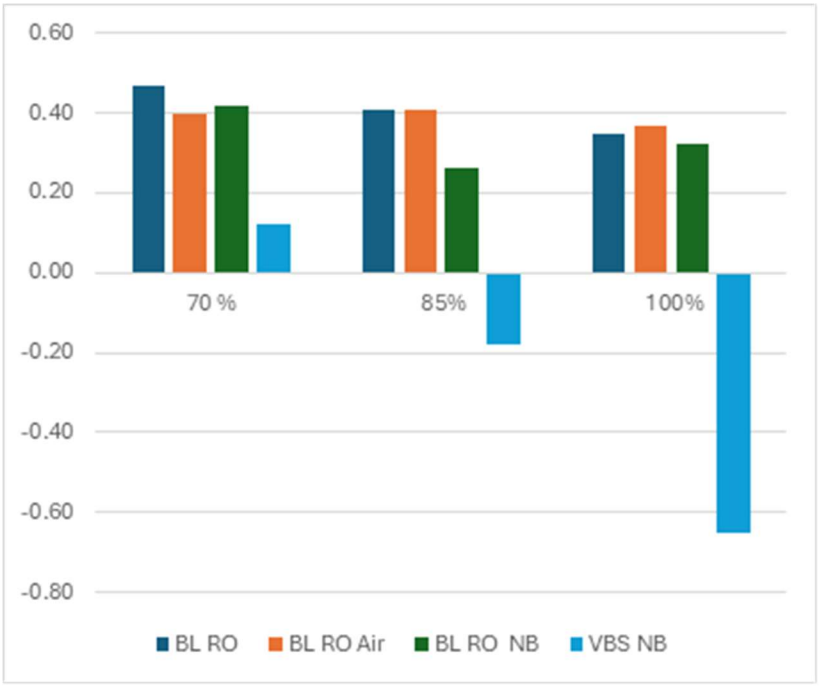

Fig. 7—Pressure fluctuation across HVS vs % flow rate.

These results show a -0.65 kPa pressure fluctuation at full tested velocity (100% flow rate) with the HVS and NB. A higher pressure drop with the HVS installed was expected because of the added restriction to the cross-sectional area. **Table 4** summarizes tubing diameters and calculations for cross-sectional and open flow areas, showing that the HVS with the barbell insert took up about ⅔ of the tubing. Given this significant constriction, a higher-pressure drop would be expected. The efficiency of vortex flow explains lower than expected pressure fluctuations. This phenomenon is not unique to this vortex experiment. Zhou et al.'s (2019) vortex study of a two-phase vortex flow tool showed a decrease in pressure drop and an increase in liquid flow.

Testing with a variety of media

Several media types were tested in the flow run, producing differing results. Media were added and tested with the HVS installed and only at inclination. Results at three flow rates and the media combinations are reflected in **Fig. 8.** Adding NB, guar and frac sand resulted in a slightly elevated pressure drop. This was expected due to the shift from water (Newtonian flow) to additives that create a non-Newtonian fluid flow environment.

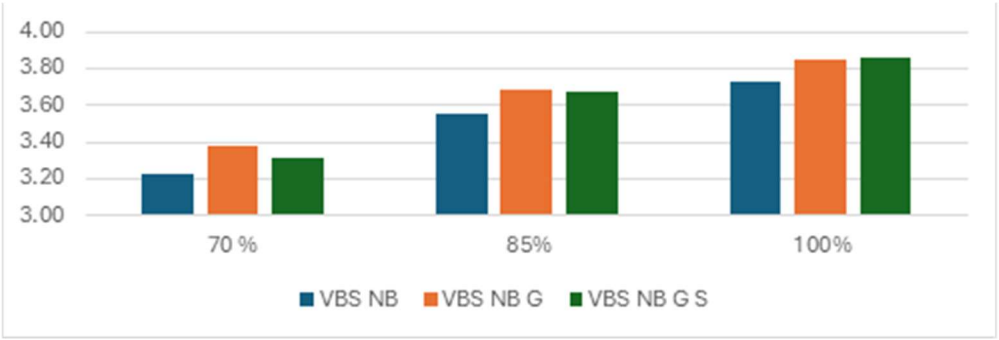

Fig. 8—Pressure differential across the HVS versus % flow rate 60° inclination.

Organized flow observed at visual fields

In addition to data findings, observations in the horizontal orientation at visual field 3, before the valve, were compared to visual field 4, situated after the valve location. Recordings from visual field 3 show erratic flow before the valve **(Fig. 9a**) and stable, organized flow after the valve (**Fig. 9b**) at visual field 4. When comparing visual fields, Fig. 9a appears erratic and irregular, with gas slugs running through the tubing. At the same time, Fig. 9b, after the HVS, shows organized flow as a regular distribution of bubbles in a spiral pattern, suggesting a vortex swirl.[4]

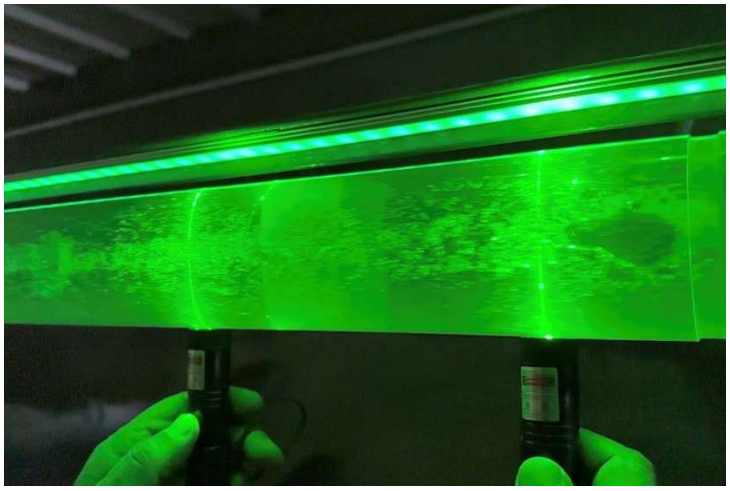

Fig. 9a—Observed erratic flow before the HVS.

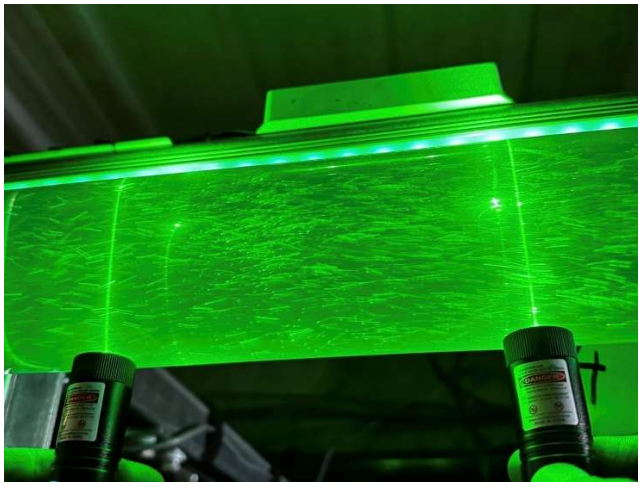

Fig 9b—Observed organized flow after HVS.

The image below at visual field 6 after the HVS (**Fig. 10**) depicts an example of air entrained in the RO water. Observations of flow at the remaining visual fields dissipated as flow progressed, while some signs of vortex structure were still visible through the middle of the ID to the end of the flow run.

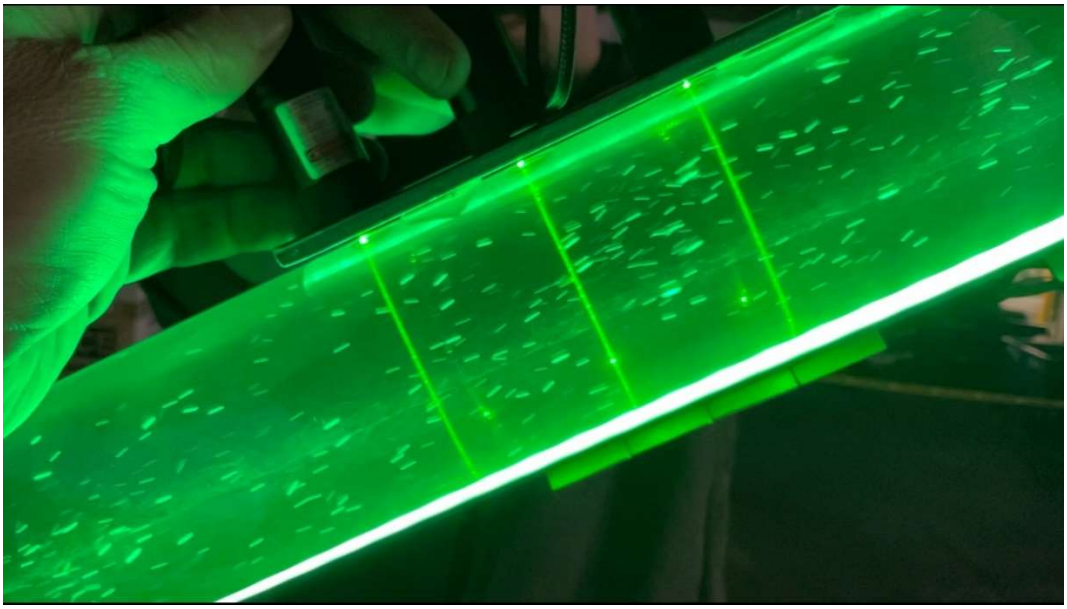

Fig. 10—Visual field 6 at 60° after the HVS.

[4] Refer to Supplementary Materials Video S-4 Baseline erratic flow and Video S-5 VBS organized flow.

Visual sinusoidal wave

Fig. 11 shows four stills taken from a single slow-motion video clip as fluid exits the HVS at visual field 6. The gas molecules that simulate the 2-dimensional sinusoidal wave trajectory demonstrate that the 3-dimensional vortex flow is intact. It was observed that in flow runs with NB, gas molecules were suspended in a sinusoidal wave vortex flow up to 25 ft away from the HVS.[5] With baseline testing (no HVS or NB), no sinusoidal wave was observed.

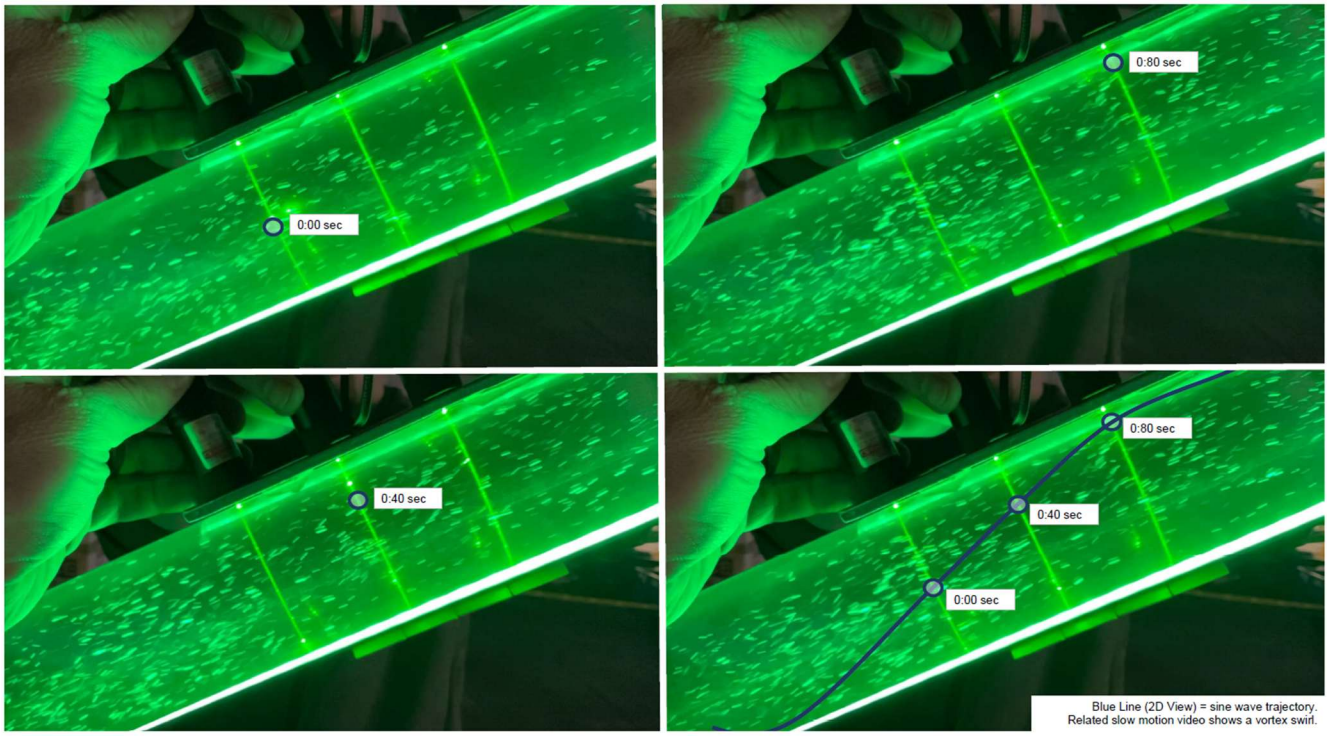

Fig. 11—Sine wave trajectory.

Reciprocation

Reciprocation with the HVS was introduced to simulate the downhole rod pumping environment. The variance between the top and bottom pressure sensors surrounding the pipe was similar on the upstroke and different on the downstroke. **Fig. 12** overlaps the top and bottom pressure sensor measurements. The dotted lines illustrate the Top Position PGauge measurements; the solid lines illustrate the Bottom Position PGauge measurements. Each pressure node is represented by a different color. The consistently lower and stable pressure readings on the bottom gauge after the HVS (PT_103 – PT_105) during deceleration suggest a vortex structure that maintains lower pressure, resisting gravity.

[5] Refer to Supplementary Materials Video S-6 Sine wave trajectory.

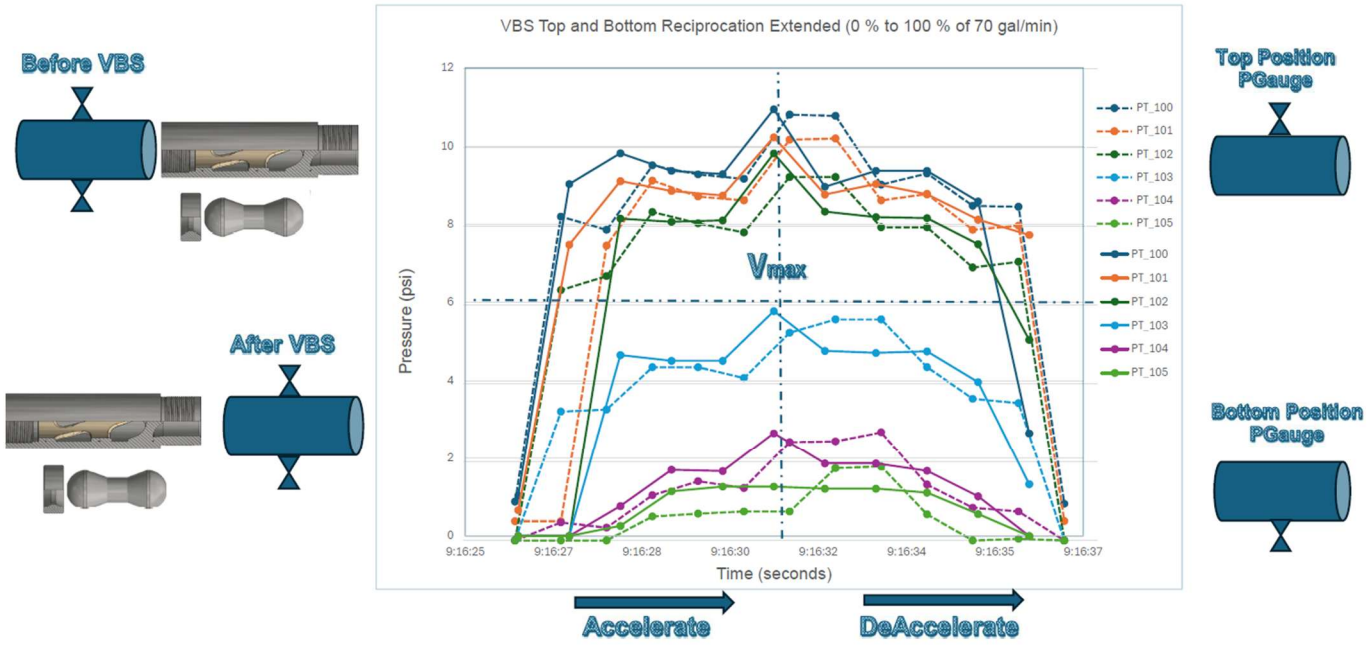

Fig. 12—Overlap of top and bottom pressure sensor measurements.

During the reciprocation simulation at a 60° incline (including HVS with NB, guar and frac sand), the differential pressures were consistent up to the maximum stroke pressure in pre- and post-HVS actuation. However, a prolonged vortex was observed during the deceleration phase of the downstroke at the bottom valve pressure sensor, indicating an intensified vortex structure attributed to flow patterns created by the HVS. The characteristics of NB and guar suspension may have prolonged the vortex structure.

Field Data Analysis

Data was gathered on HVS well installations to better understand well distribution across North America. This macro view selected data for wells in the Bakken from a southeast Saskatchewan oil producer.

Macro data analysis across North America

Enverus provided data sets from publicly available production data and well locations. **Fig. 13** below shows HVS installations across North America since 2021. Appendix E summarizes installation and operational parameters for consideration in HVS applications. These Operators reviewed and applied operational parameters appropriate to their installations and operations based on the information in Appendix E.

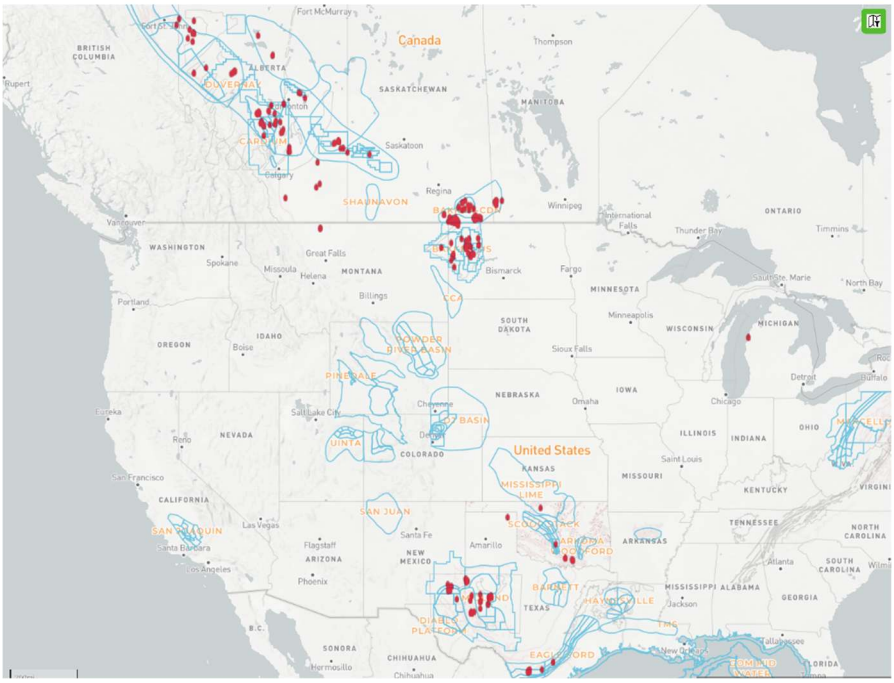

Fig. 13—HVS wells from 2021-2024 across North America.

Table 5 and **Table 6** summarize HVS installations in North America.

Country	Wells	Average TVD ft	Average MD ft
USA	160	7968	15874
CAD	181	7301	10943

Table 5—Summary of North American wells with HVS installation.

	Prod_BOE	Liquids Prod_BBL	Water Prod_BBL
Total Wells Studied	341	341	341
Total wells with production increase after HVS install	161	157	195
Percentage of ALL Wells that showed an increase	47%	46%	57%

Table 6—Data analysis of North American wells with HVS installations.

As of 2024, a single southeast Saskatchewan oil producer had 90 HVS installations in the Bakken from the North American wells shown above. This set of wells included some of Canada's highest concentrations of wells with HVS installations, providing similar well parameters for strong, comparable data microanalysis.

Microdata analysis of southeast Saskatchewan oil producer horizontal Bakken wells with HVS installations

Beginning in May 2022, a company in southeast Saskatchewan began installing HVS valves in their sucker rod pumps. Between May 2022 and April 2024, the trial was expanded to equip 90 wells with 1.25 in. and 1.5 in. HVS pump valves. The producer aimed to reduce pump failures and gas-locked pumps in wells with pumps landed at 55°-70° inclination, producing low-volume in a pumped-off state. The pumps were installed in the Torquay formation, a widespread carbonate with low permeability that requires hydraulic fracturing.

The wells had an average total vertical depth (TVD) of 7314 ft. (2230 m) and an average set depth of 7459 ft. (2274 m). The average inclination was 58.5°, and the average dog leg severity was 4.3° per 98.4 ft (30 m), with 22% of wells showing dog-leg severity equal to or greater than 7°.

A total of 90 wells were normalized for production and failure frequency data analysis. Data was categorized as pre-HVS installation and post-HVS installation.

Production Analysis

Table 7 below is a breakdown of production experienced before and after HVS installation. All wells combined showed an average increase in production after the HVS was installed, suggesting increasing pump efficiency. Data from the 90 well set was split into two sets. Seventy-six (76) of the pumps were landed at the same depth after HVS installation, and 14 wells were landed lower (in the curve) after HVS installation.

In the 14 well set, the pumps were lowered on average 722 ft (220 m) more into the curve up to a maximum of 70° inclination. Production increases on the 14 wells lowered in the curve had an average 143.5% increase in produced fluid (see **Table 7**). Landing pumps with a HVS lower into the curve reduced the producing bottomhole pressure and allowed more inflow, which increased the production volume and pump efficiency.

Well Count Analysis	* Days Post/Pre HVS	Gas Produced Gross (e^3m^3/d)	Fluid Produced (Load + Prod) (m^3)/d	Oil Produced Gross (m^3)/d	Pump Efficiency	SPM	Stroke Length (cm)
90 Wells Post HVS	127	18.89	472.80	108.12	29.45	3.58	359
90 Wells Pre-HVS	-127	14.26	357.66	87.20	20.28	3.61	357
Percent Increase/Decrease		32.5%	32.2%	24.0%	45.2%	-0.9%	0.7%
14 Wells Post Lowered HVS	136	3.70	102.97	21.28	38.19	3.94	376
14 Wells Pre-HVS	-136	1.90	42.29	8.70	18.09	3.83	367
Percent Increase/Decrease		94.7%	143.5%	144.5%	111.1%	2.9%	2.5%
76 Wells Post-HVS	127	14.88	361.51	84.66	25.49	3.43	356
76 Wells Pre-HVS	-127	12.41	316.22	78.84	20.63	3.57	355
Percent Increase/Decrease		19.9%	14.3%	7.4%	23.6%	-3.8%	0.3%

* Wells were normalized, and data was only used for equivalent well count for before and after data sets.

Table 7—Pre-and post-HVS production analysis and pump efficiency summary.

Failure Frequency Analysis

Over five years, the 90 trial wells collectively experienced 237 failures before HVS installation, with an annual failure frequency of 0.53 and an average runtime of less than 20 months between failures. A subset of 19 wells had a significantly higher annual failure frequency of 1.02 and a lower average runtime between failures of less than 12 months.

Fig. 14 depicts the breakdown of pre-HVS failure types into pump, rod, and tubing failures and illustrates a more detailed failure mechanism of the 130 pump failures. Given that all trial wells underwent hydraulic fracturing, they have the potential to produce a small amount of frac sand along with the production fluids, which leads to the prevalent issue of solids in the area. This causes premature pump valve and plunger wear, along with other mechanical issues within the insert pumps.

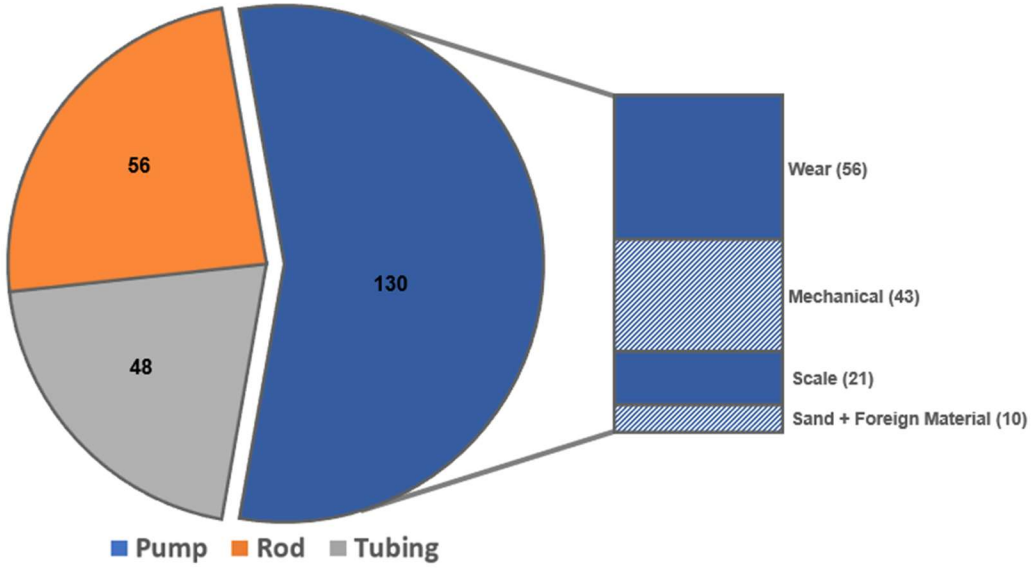

Fig. 14—Pre-HVS Failures.

After the HVS was installed on the 90 trial wells, there were 12 wells with a failure (detailed in **Table 8**), four experienced multiple failures, for a total of 16 individual failures. The failure mechanisms are detailed below. **Fig. 15** illustrates that nine wells failed due to tubing issues, four due to rod failures, and three due to pump failures. When comparing pre-HVS failures to post-HVS failure types, the distribution of failure types shifted from predominantly pump failures to tubing failures post-HVS installation.

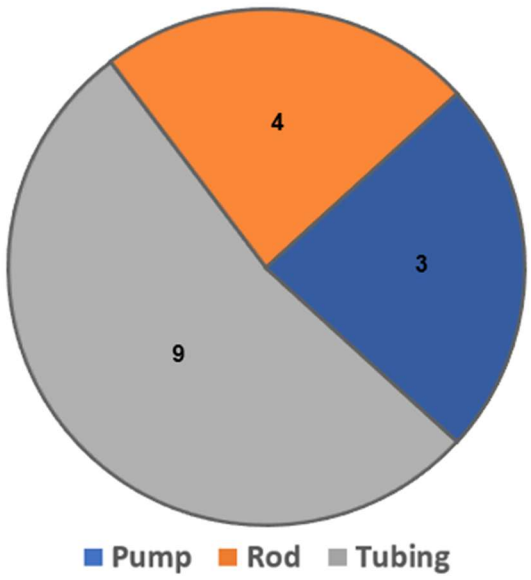

Fig. 15—Post-HVS failures.

Table 8 below summarizes individual post-HVS failures and failure mechanisms. It shows the tubing run life before the HVS pump installation. The data indicates that the tubing was approaching end-of-life or experiencing excessive wear from the wellbore trajectory, leading to failures shortly after the HVS was installed.

		First Pull		Second Pull		
HVS Run Date	Tubing Install Date	Failure Type	Failure Mechanism	Failure Type	Failure Mechanism	Notes
29-06-2022	19-09-2020	Tubing	Rod wear	Rod	Body Fatigue	Tubing had a 2-year runlife before rod failure.
28-07-2022	17-11-2015	Rod	Body Mechanical			Tubing remains in well for 9-years with no pull.
11-08-2022	11-08-2022	Tubing	MSN Wear			Tubing had a premature MSN failure.
07-09-2022	05-09-2018	Rod	Body Mechanical			Tubing remains in well for 6-years with no pull.
17-09-2022	20-09-2017	Tubing	Rod wear	Rod	Body Mechanical	Tubing had a 5-year runlife.
30-03-2023	25-09-2017	Tubing	Rod wear			Tubing had a 6-year runlife.
06-05-2023	28-08-2018	Tubing	Rod wear			Tubing had a 5-year runlife.
08-06-2023	19-12-2022	Pump	Sand			Pump was able to pump at surface.
11-07-2023	08-09-2021	Tubing	Rod wear	Tubing	Anchor Mechanical	Well trajectory has high DLS causing excessive wear.
26-09-2023	16-03-2023	Tubing	Rod wear	Tubing	Rod wear	Well trajectory has high DLS causing excessive wear.
20-10-2023	12-02-2020	Pump	Valves Worn			Pump would still pump but very low efficiency.
20-12-2023	10-09-2020	Pump	Sand			Pump was able to pump at surface.

Table 8—Post HVS failure details.

Notably, all pumps extracted for reasons other than pump failure were found to be in good condition and subsequently reinstalled. This underscores the pumps' durability, with the pump valves demonstrating resistance to abrasion from solids and corrosion within the well. Three pumps were pulled due to pump failures, and severe signs of sand production were observed. While in the well, they were seized until they were flushed with fluid to remove the solids.[6] It was speculated that the wellbore surged all the solids into the HVS at once. Once the pumps were on the surface, they could pump but were not reran due to the severe wear. With the low production volumes in these wells, sand that flows through the pump can settle back on top of the pump, making sand problems very difficult to mitigate.

The producer successfully extended the runlife of the 19 wells, with a short runlife beyond the previous failure frequency of 1.02 to 0.21. These wells continue to operate without requiring service rig intervention and are expected to continue to improve. As of Q2 2024, 15 wells (17%) in the trial have shown an extended runlife compared to the previous failure frequency. Early trends indicate that future failure frequency will continue to improve. **Fig. 16** below is a visual representation of the failure frequency improvement. The 90 wells on the Y-axis are plotted with the individual failures and HVS install date on the X-axis. This scatter plot depicts the density of failures prior to HVS installation and shows a decreased density of failures post-HVS installation.

[6] Refer to Supplementary Materials Video S-7 Solids behavior in steady state through VBS at inclination.

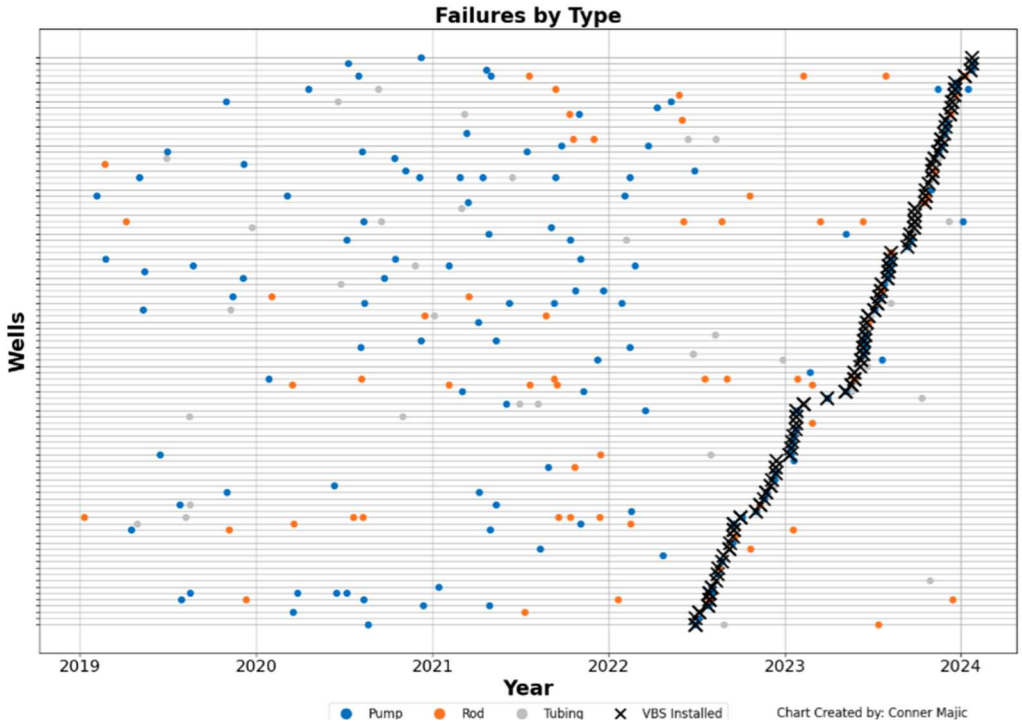

Fig. 16—Failure frequency improvement.

Conclusion

The findings presented in this paper support the effectiveness of the Hydro Dynamic System (HVS) in enhancing downhole flow dynamics through lower friction at the tubing wall, suggesting vortex flow. The most significant discovery was the HVS's hydrodynamic sealing nature at high angles.

Laboratory results with the HVS showed a hydrodynamic sealing effect, lower pressure fluctuations, and visually confirmed organized sustained vortex flow with a sinusoidal wave structure. This would explain why the HVS operates well at inclinations between 55°-70° in field trials and 90° in the lab. During the deceleration portion of reciprocation testing, pressure sensors on the bottom of the tubing consistently measured lower pressure fluctuations after the HVS with respect to measurements at the top of the tubing. This indicates decreased friction, suggesting vortex flow; thereby, resulting in lower friction on the tubing wall.

Laboratory analyses related to the field study, which consistently demonstrated that the introduction of the HVS performs at high angle inclination, allowing operators to venture deeper into wellbores toward primary horizontal reservoirs to gain production uplift. In particular, the 14 wells (Table 6) lowered to a 70° angle exhibited a 143.5% increase in production, highlighting the HVS's effectiveness in optimizing flow conditions at higher inclinations and lower depths.

These findings challenge conventional ball and seat traveling and standing valves. They open avenues for further research into advanced systems that use hydrodynamic force to seal in reciprocating downhole environments and enhance the potential of the HVS in achieving effective sealing to reduce failure frequency, promoting pump longevity when pumping around the curve.

Acknowledgements

The authors thank their respective companies for permission to author and publish this collaborative paper. We extend our gratitude to Q2 Artificial Lift Systems and Doug Quinn for providing funding, space and time to erect the flow run apparatus and conduct run testing. Our thanks to Veren and Enverus for supplying and analyzing field data and to Dr. Al Darzins of Nano Gas Environmental for supplying the Unit L6 Nanobubble Generator verification data.

References

Aslanov, H. 2024. Development of downhole pump valve assembly. ETM-Equipment Technologies Materials 02 (20): 132-139. https://doi.org/10.36962/etm20022024-132.

Connally, C., Sandberg, C., and Stein, N. 1953. Volumetric Efficiency of Sucker Rod Pumps When Pumping Gas-Oil Mixtures. Journal of Petroleum Technology 5 (10): 265-270. https://doi.org/10.2118/284-G.

Coyes, C., Williams, B., Jensen, C., Conner, M., Link, B., Saponja, J., Quinn, J. 2023. Implementation of a New Proprietary Vortex Fluid Sucker Rod Pump System to Improve Production by Enhancing Flow Dynamics. SPE Production & Operations 38 (04): 578–589. SPE-206908-PA. https://doi.org/10.2118/206908-PA.

Jalikop, S., Scheichl. B., Eder, J. and Stefan, H. 2020. Computational Fluid Dynamics Model to Improve Sucker Rod Pump Operating Mode. Presented at the SPE Annual Technical Conference and Exhibition, Virtual, October 2020. SPE Annual Technical Conference and Exhibition. SPE-201285-MS. https://doi.org/10.2118/201285-MS.

Jegbefume, O., Bang, J., Ledroz, A., Shoup, R., Vincent, R. and Earley, J. August 2018. Rod-Guide Placement Based on High-Resolution Tortuosity Analysis of Production Tubing. Paper presented at the SPE Artificial Lift Conference and Exhibition - Americas, The Woodlands, Texas, USA, August 2018. SPE-190935-MS. https://doi.org/10.2118/190935-MS.

Kolawole, O., Gamadi T., and Bullard, D. October 2019. Comprehensive Review of Artificial Lift System Applications in Tight Formations. Paper presented at the SPE Eastern Regional Meeting, Charleston, West Virginia, USA, October 2019. SPE-196592-MS. https://doi.org/10.2118/196592-MS.

Luo, X., Yang, L., Yin, H., He, L., and Lü, Y. 2019. A review of vortex tools toward liquid unloading for the oil and gas industry. *Chemical Engineering and Processing - Process Intensification* **145**: 107679. https://doi.org/10.1016/j.cep.2019.107679.

Mingaleeva, G. 2002. On the Mechanism of a Helical Motion of Fluids in Regions of Sharp Path Bending. *Technical Physics Letters* **28** 657-659. https://doi.org/10.1134/1.1505541.

Ohgaki, K., Khanh, N., Joden, Y., Tsuji, A. and Nakagawa, T. 2010. Physicochemical approach to nanobubble solutions. *Chemical Engineering Science* **65** (3): 1296-1300. https://doi.org/10.1016/j.ces.2009.10.003.

Saponja, J., Kubacak, T. and Nagoo, A. 2023. Rod Pumping the Curve to Maximize Drawdown and Control Slugging. *Southwestern Petroleum Short Course*. Lubbock, Texas. https://www.swpshortcourse.org/papers?combine=trey&items_per_page=25.

Walke, S. and Sathe, V. 2012. Experimental Study on Comparison of Rising Velocity of Bubbles and Light Weight Particles in the Bubble Column. *International Journal of Chemical Engineering and Applications* **3** (1): 25-30. https://doi.org/10.7763/IJCEA.2012.V3.153.

Zhou, C., Wu, X., Zhang, T., Zhao, X., Gai, S. and Xiang, H. 2019. Dynamic analysis for two-phase vortex flow and optimization of vortex tools. *Journal of Petroleum Science and Engineering* **173**: 965-974. https://doi.org/10.1016/j.petrol.2018.10.091.

Zhou, L., Wang, S., Zang, L., and Hu, J. 2021. Generation and Stability of Bulk Nanobubbles: A Review and Perspective. *Current Opinion in Colloid & Interface Science* **53**. https://doi.org/10.1016/j.cocis.2021.101439.

Appendix A: Laboratory Flow Run Apparatus - Horizontal

Pressure Sensors	Horizontal	VBS Placement
S1 – S2	73 in.	
S2 – S3	156 in.	78 in.
S3 – S4	73 in.	
S4 – S5	147 in.	
S5 – S6	292 in.	

Table A1—Distance between pressure sensors and VBS in horizontal orientation.

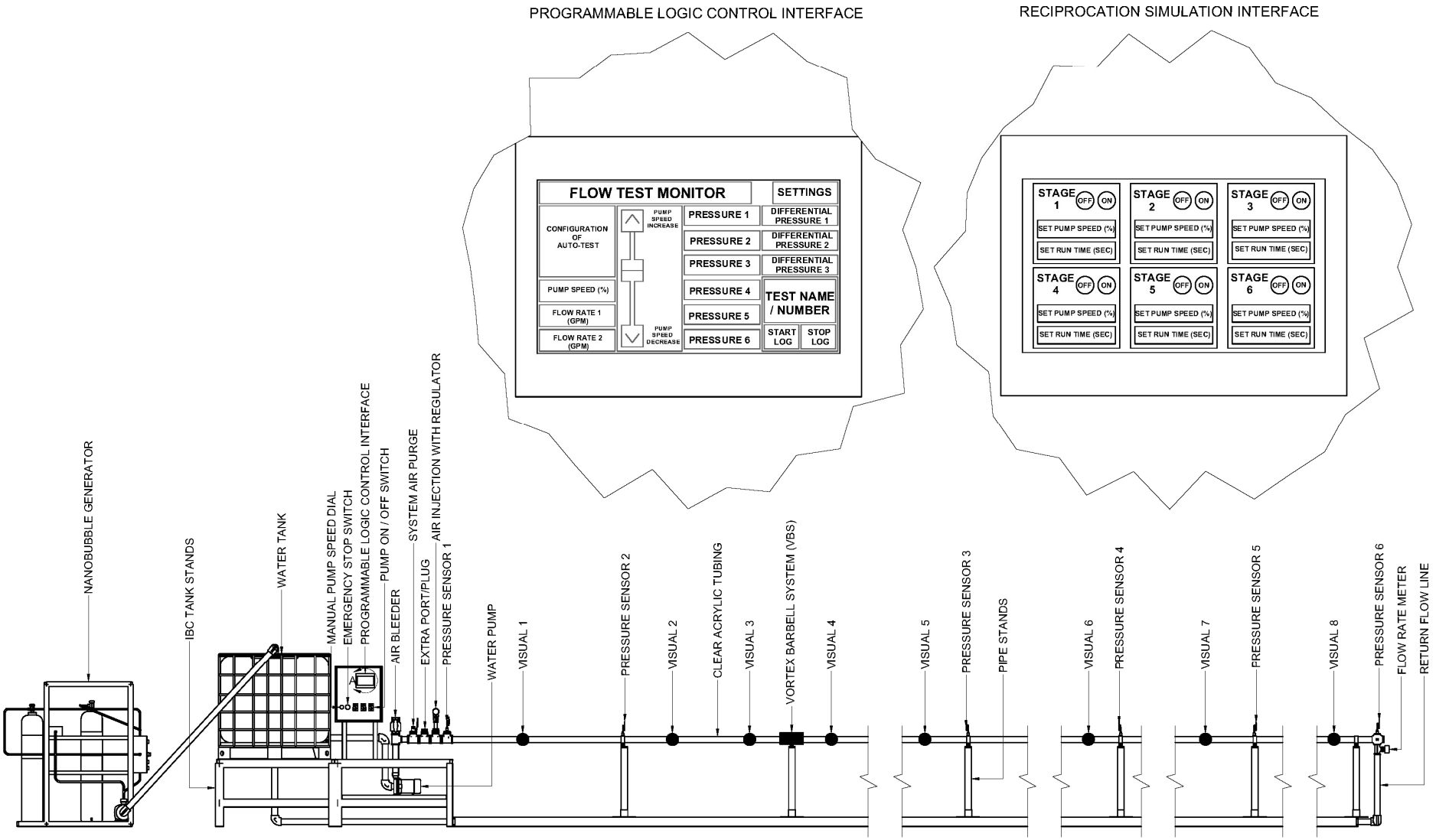

Fig. A1—Laboratory flow run apparatus, horizontal.

Appendix B: Laboratory Flow Run Apparatus – Incline

Pressure Sensors	Incline	VBS Placement
S1 – S2	224 in.	
S2 – S3	160 in.	
S3 – S4	156 in.	78 in.
S4 – S5	147 in.	
S5 – S6	73 in.	

Table A2—Distance between pressure sensors and VBS at an incline.

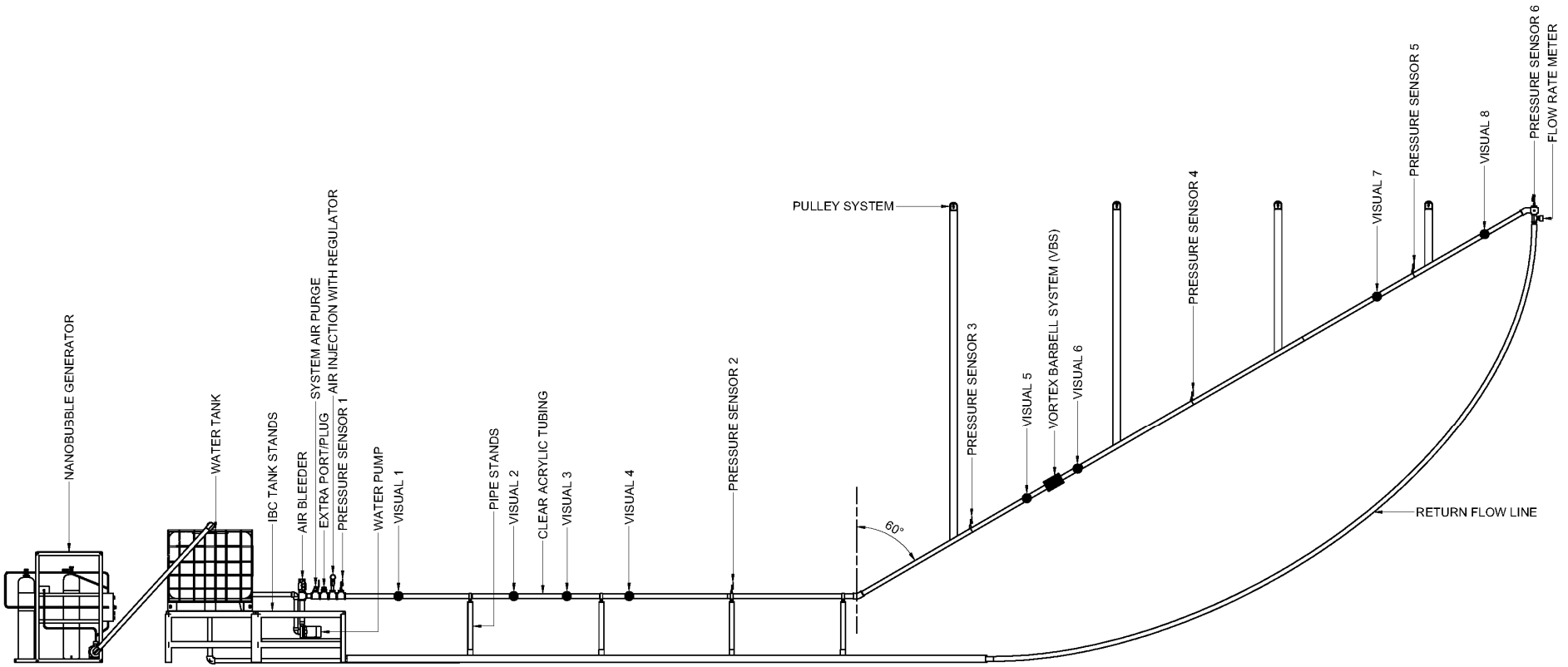

Fig. A2—Laboratory flow run apparatus, incline.

Appendix C: Laboratory Apparatus Component Specifications

Product name	Manufacturer	Technical specifications
Compact Rugged Pressure Transmitter PX119 Series	Omega	0.50% Best Fit Straight Line (BFSL) Accuracy Stainless Steel Body Pressure Range: 15 to 5000 psi (345 bar) Output: 4 to 20 mA, 0 to 5 Vdc Process Connection: 1/8 NPT Male Response Time: 1 ms
X7 Micro OCS (Input/Output Controller) PLC	Horner Automation Group	Touchscreen User Interface Control Programmable Screens Multiple Inputs and Outputs Data Logging Capabilities
2 in. Digital Turbine Flow Meter	YFIXTOOL	LCD Digital Display Flow Rate 60-500 LPM (15-132 GPM) Accuracy of +/- 1% Instantaneous and Cumulative Flow Readings
Long Range Tactical Green Beam Flashlight	Gniby	high powered green light laser
LED Strip Lights	LED World	Multiple color control and brightness selection
Pump Specifications	Franklin Electric	Model: FBSE-150-S HP: 1.5 Volts: 150/230 V
Pump Motor	TechTop	Model: JEP0012DP HP: 1.5 RPM: 3500 Voltage: 230/460 V
VFD	TechTop	Model: TD350-2R2G-2 HP: 3 Voltage: 220 V

Table A3—Flow run component specifications.

Appendix D: Nanobubble Generator Verification

The Nanobubble Generator was verified as part of the nanobubble generator operator's verification process. Unit L6, used in this experiment, was verified on February 2022 using Malvern Panalytical's (Malvern, UK) NanoSight N300 instrument housed in Northwestern University's International Institute of Nanotechnology in Evanston Illinois. Verification testing was conducted by Dr. Al Darzins of Nano Gas Environmental.

Results from Unit L6 verification are shown in **Fig. A3** below with air at 100 psi. The vertical blue line shows concentrations of nanobubbles produced under 350 nm to achieve changes in physicochemical properties that support the production of a double slip layer to reduce turbulence and friction.

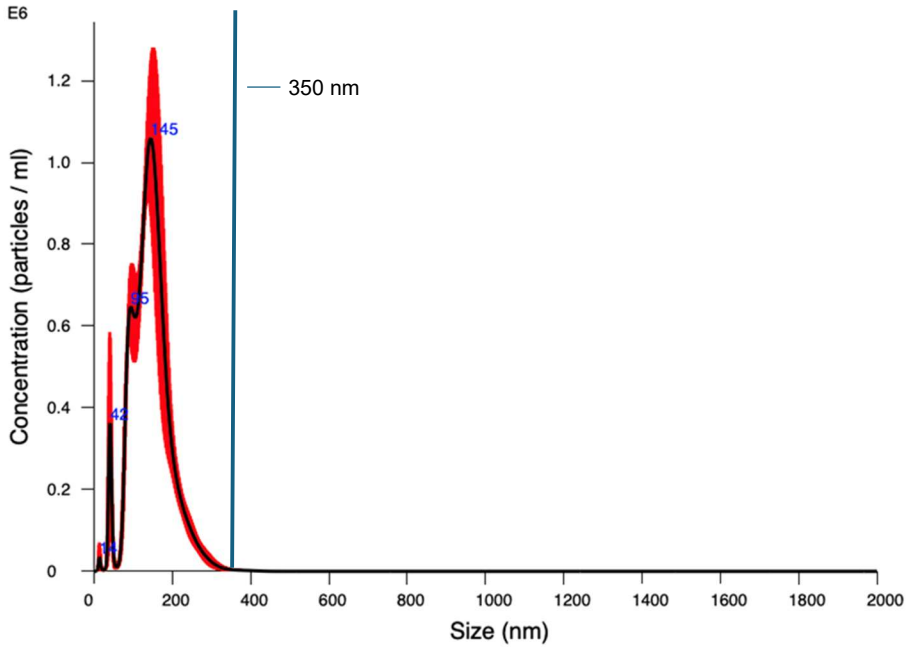

Fig. A3—Nanobubble generator verification, Unit L6

Appendix E: Hydro Dynamic System Optimization

HVS systems are reliant on the components that surround them. Recommendations for systems used in the field trials were extracted from Q2-Trak™ software. HVS installations included, with some variance, the following:

1. Cleaning the well out before sumping the pump, if possible
2. Pump landing area – avoid doglegs (Jegbefume et al., August 2018)
3. Stiff rods with more guides and additional sinker bars for weight (Jegbefume et al., August 2018)
4. Valve rod guide hardness
5. Pull tube guides (greater surface area for wear)
6. Vortex sand-check device in the curve to protect the plunger barrel.
7. Hardened grooved plunger
    a. Looser fit plungers (i.e., 8 to 12 thou size below base or clearance)
    b. Shorter plungers (as to not have too much deflection in the barrel)
    c. Higher interference ring (frac sand plunger).
8. HVS travelling valve
9. Optimized barrel metallurgy
10. HVS standing valve
11. Low friction / low-pressure drop strainer
12. Dual intake eccentric gas separator (Saponja et al. 2023)
13. High annular flow-by cross-sectional area eccentric tubing anchor
14. Start-up procedures – back pressure on the system
15. Rod rotator
16. Optimize POC (pump off controller) and VFD (variable frequency drive)
17. Re-space travel valve to increase compression ratio (~2 weeks post start-up)
18. Consider eccentric tubing anchor higher in the hole to have gas escape the tubing (Saponja et al. 2023)